Dependence of crystal orientation in Al-induced crystallized poly-Si layers on SiO_2 insertion layer thickness

Atsushi Okada[a], Kaoru Toko[a], Kosuke O. Hara[b], Noritaka Usami[b,c], and Takashi Suemasu[a,b]

[a]*Institute of Applied Physics, University of Tsukuba, 1-1-1 Tennodai, Tsukuba, Ibaraki 305-8573, Japan*

[b]*Japan Science and Technology Agency, CREST, 5, Sanbancho, Chiyoda-ku, Tokyo 102-0075, Japan*

[c]*Institute for Materials Research, Tohoku University, 2-1-1, Katahira, Aoba-ku, Miyagi 980-8577, Japan*

We have fabricated poly-Si thin films on fused silica substrates by the Al-induced crystallization (AIC) method with SiO_2 insertion layers of various thicknesses (0-20 nm). The growth morphologies of poly-Si layers were dramatically changed by the SiO_2 thickness, *i.e.,* thin layers (2 nm) provided high growth rates and (100) orientations, and thick layers (10 nm) provided low growth rates and (111) orientations. These results showed that the crystal orientation of AIC-Si significantly depends on the diffusion rate of Si atoms into the Al layer.

PACS: 61.05.cp; 61.05.jh; 68.55.ag

Keywords: A1. Growth models; A3. Solid phase epitaxy; B2. Semiconducting silicon; B3. Solar cells

1. Introduction

The Al-induced crystallization (AIC) method is known as a method for obtaining thin poly-Si layers on glass substrates, where amorphous Si (a-Si) layers on Al are transformed into a crystalline phase via exchange between the Al and Si layers during annealing [1]. This method enables us to fabricate seed layers for epitaxially grown absorbers for thin-film solar cells on inexpensive SiO_2 substrates [2-7]. Conventional solid phase crystallization (SPC) requires temperatures higher than 600°C, and the Si grains obtained are as small as a few μm [8]. In the AIC method, Si crystallizes at relativity low temperatures in the range of 400-500°C, and large grains of tens of μm in size can be obtained even on non-lattice-matched substrates [9,10]. Therefore, the Si seed crystals fabricated by the AIC method seem to enable the growth of high-quality devices such as thin-film solar cells and thin-film transistors on low-cost glass substrates [11-15]. The crystal orientation is critical for device performances [16]. Thus, the control of crystal orientations in the poly-Si layers is required.

However, factors determining the preferential crystal orientation of AIC-Si layers remain an open question. Preferential (100) orientation of the AIC-Si layers has been reported [9,13,17]. On the other hand, growth of (111)-oriented Si layers has been also reported [15,18]. Kurosawa *et al.* showed that the preferential orientation of AIC-Si on fused silica can be controlled by changing the exposure time of Al in air, and they proposed

46 a model showing that the orientation of AIC-Si is determined by the crystal phase of the
47 native Al oxide [19]. In contrast, Jung *et al*. considered that the preferential orientation
48 depends on the annealing temperature, and proposed a model showing that the growth rate
49 of AIC-Si determines the preferential orientation [20]. In this study, our aim was to
50 investigate the influence of Si diffusion rate on the preferential orientation of AIC-Si. We
51 also aimed to develop a method to control the crystal orientation of AIC-Si. For this purpose,
52 we introduced SiO_2 layers with various thicknesses as intermediate layers between the a-Si
53 and Al layers and carried out the AIC method. The SiO_2 layer thickness is easier to control
54 compared to the thickness of a native Al oxide. In addition, the effect of the intermediate
55 layer crystallinity on the AIC-Si is negligible when we discuss the crystal orientation of
56 AIC-Si layers.

57

58 **2. Experimental procedures**

59 Fused silica wafers were used as substrates in this work. A 100-nm-thick Al film was
60 sputtered at room temperature (RT) on the substrate. Next, an amorphous SiO_2 layer was
61 subsequently sputtered at RT on the Al layer, followed by sputtering a 100-nm-thick a-Si
62 film at RT without breaking the vacuum. The thickness of the SiO_2 layer was varied from 0
63 to 20 nm. All the depositions were carried out by radio-frequency (RF) magnetron
64 sputtering. For comparison, conventional AIC method was also performed, that is,

65 deposition of Al layers, followed by breaking the vacuum to form a native Al layer for 48 h,
66 and the subsequent deposition of a-Si layers. The argon pressure during the sputtering was
67 0.2 Pa. The RF power was set at 100 W. The AIC method was carried out by annealing the
68 samples in N_2 atmosphere at 500 °C for 10 h. Sample preparation was summarized in Table
69 1. The surface morphologies of some of the samples were observed during annealing by
70 optical microscopy. After annealing, the Al and oxide layers were etched away using a HF
71 solution (HF: 2%). The crystal orientation of AIC-Si was characterized by electron
72 backscatter diffraction (EBSD) measurement.
73

74 **3. Results and discussion**

75 The time evolution of optical microscope images for sample D, prepared with a
76 2-nm-thick SiO_2 intermediate layer, is shown in Figs. 1(b)-1(e), and those for sample H,
77 prepared with a 10-nm-thick SiO_2 layer, are shown in Figs. 1(f)-1(i). Figure 1(a) shows the
78 expected schematic cross-sectional diagram of each crystallization stage. Upon heating,
79 interdiffusion of Al and Si atoms begins. After the diffused atoms become supersaturated,
80 they begin to nucleate. The time necessary for Si nuclei to be observed with an optical
81 microscope is defined as the incubation time. After that, these nuclei were grown laterally.
82 The change of Si crystal radius per unit time is defined as growth rate. In growth stage, few
83 nuclei were generated. The dependence of the incubation time and growth rate on the

84 thickness of the SiO_2 intermediate layer is shown in Fig. 2. The results for sample I were
85 excluded as described later. This graph shows that the thicker the SiO_2 intermediate layer,
86 the longer the incubation time and the smaller the growth rate. This means that the SiO_2
87 intermediate layer works as a diffusion barrier for Si atoms, which is supported by the fact
88 that the diffusion coefficient of Si in SiO_2 is approximately 1000 times smaller than that in
89 Al [21,22]. On the basis of the results shown in Fig. 2, it can safely be stated that the
90 diffusion rate of Si depends on the SiO_2 intermediate layer thickness.

91 Figure 3 shows the crystal orientation mappings obtained by EBSD for AIC-Si layers
92 fabricated with various SiO_2 intermediate layer thicknesses. When we employed the
93 conventional AIC method, highly (111)-oriented AIC-Si layers were formed in sample A as
94 shown in Fig. 3(a). We next discuss the influence of SiO_2 intermediate layer thickness on
95 the AIC-Si crystal orientation. As shown in Figs. 3(b) and 3(f), the grain size of AIC-Si is
96 considerably small, less than 1 μm both when the SiO_2 intermediate layer thickness is zero
97 (sample B) and when it is very thick (20 nm, sample I). In the case of AIC-Si formed
98 without the SiO_2 layer as in sample B, the Si atoms were thought to diffuse into the Al
99 layer very rapidly, causing supersaturation shortly upon heating, and thus the Si atoms
100 started to nucleate everywhere at the Si/Al interface, resulting in small grains as shown in
101 Fig 3(b). In the case of very thick SiO_2 layer (20 nm, sample I), the results have not been
102 completely understood. In general, sputtered SiO_2 films contain a certain amounts of

103 defects [23]. We speculate that these defects might significantly influence the diffusion of
104 Si atoms and thereby generation of Si nuclei at the Al/SiO_2 interface, making it difficult to
105 understand the AIC process by the simple model shown in Fig. 1. In contrast, when the
106 SiO_2 intermediate layer was 2-10 nm in thickness (samples C-H), the AIC-Si grains
107 exceeded tens of μm in size as shown in Figs. 3(c)-3(e). We think that the Si diffusion was
108 suppressed moderately by this SiO_2 layer, and thus only a small number of Si nuclei were
109 generated at the Al/SiO_2 interface, leading to lateral growth of Si nuclei as shown in Figs.
110 3(c)-3(e). Figure 4 shows the SiO_2 intermediate layer thickness dependence of crystal
111 orientation fractions of Si. The results obtained for sample I were not included. When the
112 SiO_2 intermediate layer was 1 nm thick, the AIC-Si became highly (100) oriented. On the
113 other hand, highly (111)-oriented AIC-Si layers were formed when the SiO_2 intermediate
114 layer was 10 nm thick. The crystal orientation was determined from grains whose
115 misorientation from the ideal (100) and (111) planes was less than 10°. The areas other
116 than the (100) and (111) planes were much smaller, and thus were excluded in Fig. 4.
117 These results suggest that the orientation of a poly-Si thin film fabricated by the AIC
118 method depends significantly on the SiO_2 layer thickness, thereby the diffusion rate of Si.
119 Next, we discuss the mechanism of preferential AIC-Si crystal orientation dependence
120 on the SiO_2 intermediate layer thickness, and thus the diffusion rate of Si atoms to the Al
121 layer. The surface energy in crystalline Si is the lowest for the (111) plane, followed by the

122 (100) plane [24]. We think that the crystal plane dependence of the interface energy at the
123 crystalline Si/amorphous SiO_2 interface is mostly the same as that in the crystalline Si,
124 because SiO_2 has no anisotropy. The growth rate in Si is the largest on the (100) plane [25].
125 The nucleation of Si occurs at the Al/SiO_2 interface in AIC, because the concentration of Si
126 is the largest there within the Al layer. When the SiO_2 intermediate layer is thick and the Si
127 diffusion rate is small, the concentration of Si in the Al increases gradually. Therefore, in
128 the nucleation stage, only the most stable nuclei, (111)-oriented Si nuclei, are generated. In
129 the crystal growth stage, these (111)-oriented nuclei grow laterally. As a result, the poly-Si
130 film becomes (111) oriented. This (111) domination appears to contradict the theory
131 presented by Schneider *et al* [26]. This contradict is possibly originated from the difference
132 in the Al and Si thicknesses, because these thicknesses significantly affect the orientation
133 of the AIC-Si layer [27]. In contrast, when the SiO_2 intermediate layer is thin and the Si
134 diffusion rate is large, the degree of supersaturation is likely to become large. Therefore, in
135 the nucleation stage, (100)-oriented nuclei, the second most stable nuclei, are generated in
136 addition to the (111)-oriented nuclei. In the crystal growth stage, (100)-oriented nuclei
137 grow rapidly because these grains have (100) facets. Therefore, (100)-oriented nuclei
138 finally become dominant.
139

140 **4. Conclusions**

In summary, we have fabricated poly-Si thin films on fused silica substrates by the AIC method using SiO_2 intermediate layers with various thicknesses (0-20 nm) between the a-Si (100 nm) and Al (100 nm) layers. The incubation time and growth rate of the Si grains depended on the SiO_2 layer thickness. With increasing SiO_2 layer thickness from 2 to 10 nm, the crystal orientation of the AIC-Si changed gradually from the (100) to (111) orientation. This selective formation technique of (100) and (111) oriented poly-Si films opens up a possibility of high-quality epitaxial templates for thin film devices.

Acknowledgments

This work was financially supported by Japan Science and Technology Agency, CREST and Grant-in-Aid for Research Activity Start-up (No. 23860011 MEXT). A part of this work was conducted by the AIST Nano-Processing Facility, supported by "Nanotechnology Network Japan" of MEXT, Japan.

155 **References**

156 [1] O. Nast, T. Puzzer, L. M. Koschier, A. B. Sproul, and S. R. Wenham, Appl. Phys. Lett. 73
157 (1998) 3214.

158 [2] Z. Shi and M. A. Green, Prog. Photovoltaics 6 (1998) 247.

159 [3] P. I. Widenborg and A. G. Aberle, J. Cryst. Growth 242 (2002) 270.

160 [4] E. Pihan, A. Slaoui, and C. Maurice, J. Cryst. Growth 305 (2007) 88.

161 [5] H. Kuraseko, N. Orita, H. Koaizawa, and M. Kondo, Appl. Phys. Express 2 (2009)
162 015501.

163 [6] I. Gordon, L. Carnel, D. Van Gestel, G. Beaucarne, and J. Poortmans, Thin Solid Films
164 516 (2008) 6984.

165 [7] B. R. Wu, S. Y. Lo, D. S. Wuu, S. L. Ou, H. Y. Mao, J. H. Wang, and R. H. Horng, Thin
166 Solid Films 520 (2012) 5860.

167 [8] R.B. Bergmann, G. Oswald, M. Albrecht, and V. Gross, Sol. Energy Mater. Sol. Cells 46
168 (1997) 147.

169 [9] H. Kim, D. Kim, G. Lee, D. Kim, and S. H. Lee, Sol. Energy Mater. Sol. Cells 74 (2002)
170 323.

171 [10] S. Gall, M. Muske, I. Sieber, O. Nast, and W. Fuhs, J. Non-Cryst. Solids 299-302 (2002)
172 741.

173 [11] Y. Ishikawa, A. Nakamura, Y. Uraoka, and T. Fuyuki, Jpn. J. Appl. Phys. 43 (2004) 877.

174 [12] I. Gordon, L. Carnel, D. Gestel, G. Beaucarne, and J. Poortmans, Prog. Photovoltaic 15
175 (2007) 575.
176 [13] P. Prathap, O. Tuzun, D. Madi, and A. Slaoui, Sol. Energy Mater. Sol. Cells 95 (2011)
177 S44.
178 [14] K. Toko, M. Kurosawa, H. Yokoyama, N. Kawabata, T. Sakane, Y. Ohta, T. Tanaka, T.
179 Sadoh, and M. Miyao, Appl. Phys. Express 3 (2010) 075603.
180 [15] D. Tsukada, Y. Matsumoto, R. Sasaki, M. Takeishi, T. Saito, N. Usami, and T. Suemasu,
181 Appl. Phys. Express 2 (2009) 051601.
182 [16] S. M. Sze, Physics of Semiconductor Devices, p. 386, 2nd ed. (Wiley, New York, 1981)
183 [17] S. Gall, J. Schneider, J. Klein, K. Hübener, M. Muske, B. Rau, E. Conrad, I. Sieber, K.
184 Petter, K. Lips, M. Stöger-Pollach, P. Schattschneider, and W. Fuhs, Thin Solid Films
185 511-512 (2006) 7.
186 [18] Y. Sugimoto, N. Takata, T. Hirota, K. Ikeda, F. Yoshida, H. Nakashima, and H.
187 Nakashima, Jpn. J. Appl. Phys. 44 (2005) 4770.
188 [19] M. Kurosawa, N. Kawabata, T. Sadoh, and M. Miyao, Appl. Phys. Lett. 95 (2009)
189 132103.
190 [20] M. Jung, A. Okada, T. Saito, T. Suemasu, and N. Usami, Appl. Phys. Express 3 (2010)
191 095803.
192 [21] S. Fujikawa, K. Hirano, and Y. Fukushima, Metall. Trans. A 9A (1978) 1811.

193 [22] S. Fukatsu, T. Takahashi, and K. M. Itoh, Appl. Phys. Lett. 83 (2003) 3897.

194 [23] Y. Urabe, T. Sameshima, K. Motai, and K. Ichimura, Jpn. J. Appl. Phys. 47 (2008) 8003.

195 [24] A. A. Stekolnikov, J. Furthmuller, and F. Bechstedt, Phys. Pev. B 65 (2002) 115318.

196 [25] L. Csepregi, E. F. Kennedy, and J. W. Mayer, J. Appl. Phys. 49 (1978) 3906.

197 [26] J. Schneider, A. Sarikov, J. Klein, M. Muske, I. Sieber, T. Quinn, H.S. Reehal, S. Gall,

198 and W. Fuhs, J. Crystal Growth 287 (2006) 423.

199 [27] M. Kurosawa, K. Toko, N. Kawabata, T. Sadoh, and M. Miyao, Solid-State Electron. 60

200 (2011) 7.

201

202 Fig. 1 (a) Schematic cross-sectional diagrams of each crystallization stage, optical
203 micrographs of surface morphologies of sample D, prepared with a 2-nm-thick SiO_2
204 intermediate layer, after annealing for (b) 40, (c) 50, (d) 55, and (e) 60 min, and those for
205 sample H, prepared with a 10-nm-thick SiO_2 intermediate layer after annealing for (f) 120, (g)
206 150, (h) 180, and (i) 210 min.

207

208 Fig. 2 Dependence of the incubation time and growth rate on the SiO_2 intermediate layer
209 thickness.

210

211 Fig. 3 Dependence of crystal orientation mappings of AIC-Si on the SiO_2 intermediate layer
212 thickness for (a) sample A (native Al-oxide), (b) sample B (0 nm), (c) sample D (2 nm), (d)
213 sample G (5 nm), (e) sample H (10 nm), and (f) sample I (20 nm).

214

215 Fig. 4 Dependence of AIC-Si crystal orientation fractions on the SiO_2 intermediate layer
216 thickness.

217

Table 1 Preparation of samples A-I. Al layer thickness, air exposure time, SiO_2 and a-Si layer thicknesses are shown.

Sample	Al (nm)	Air exposure (h)	SiO_2 (nm)	Si (nm)
A	100	48	0	100
B	100	0	0	100
C	100	0	1	100
D	100	0	2	100
E	100	0	3	100
F	100	0	4	100
G	100	0	5	100
H	100	0	10	100
I	100	0	20	100

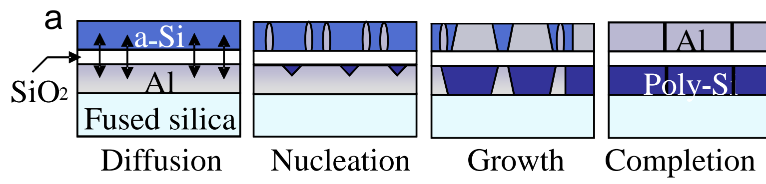

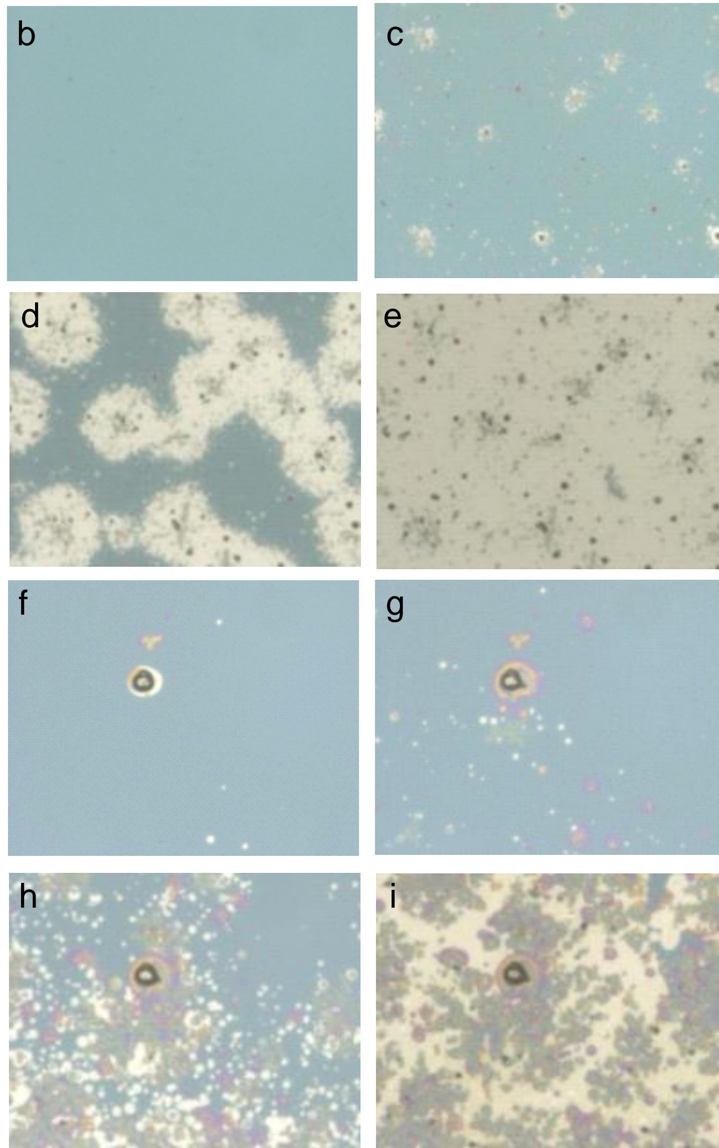

Figure 1

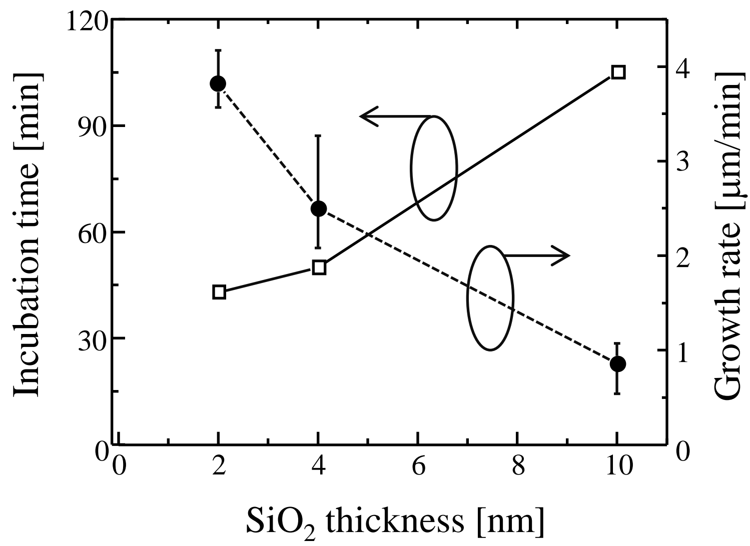

Figure 2

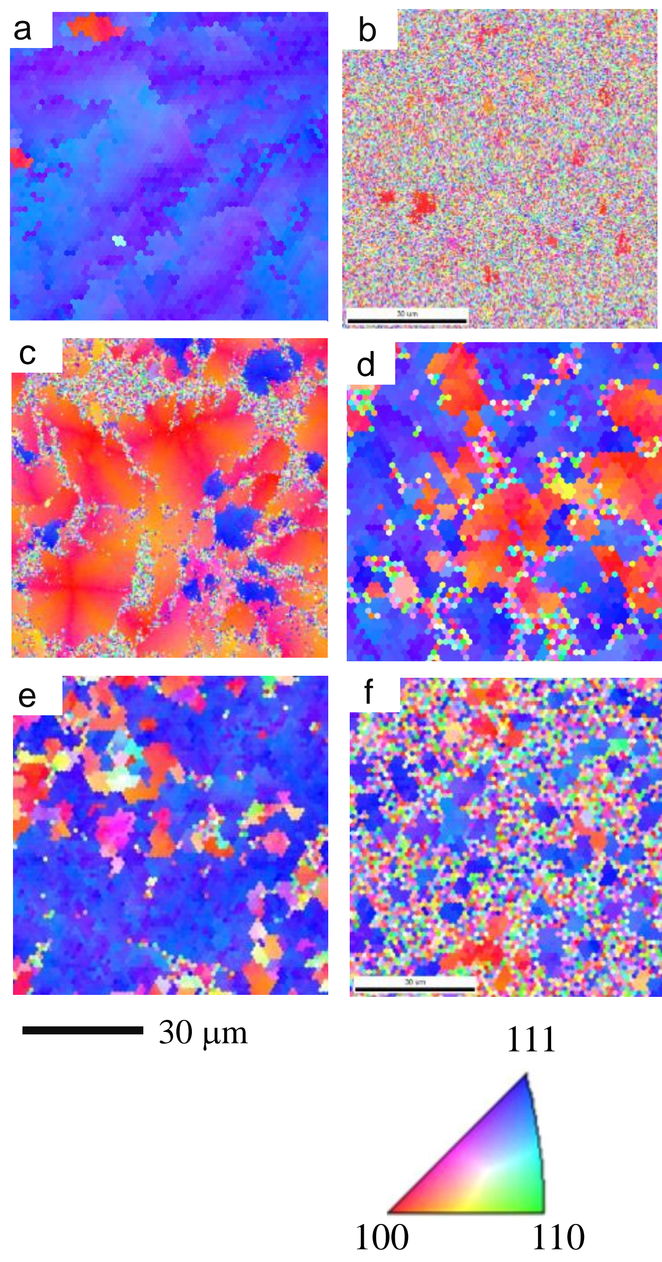

Figure 3

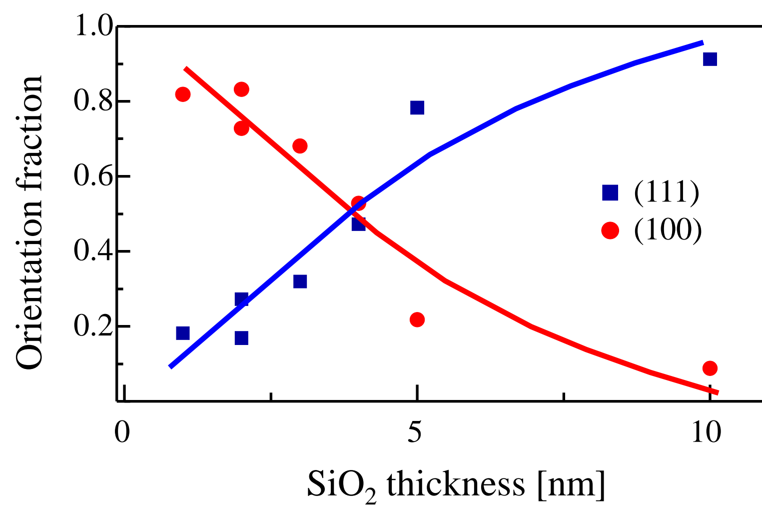

Figure 4